Graphene Field-Effect Transistors on Undoped Semiconductor Substrates for Radiation Detection

Michael Foxe, *Student Member, IEEE*, Gabriel Lopez, *Student Member, IEEE*, Isaac Childres, Romaneh Jalilian, Amol Patil, Caleb Roecker, John Boguski, Igor Jovanovic, and Yong P. Chen, *Member, IEEE*

***Abstract*—The use of a graphene field-effect transistors (GFETs) to detect radiation is proposed and analyzed. The detection mechanism used in the proposed detector architecture is based on the high sensitivity of graphene to the local change of electric field that can result from the interaction of radiation with a *gated undoped* semiconductor absorber (substrate) in a GFET. We have modeled a GFET-based radiation detector, and discussed its anticipated performance and potential advantages compared to conventional detector architectures.**

***Index Terms*—FET, graphene, graphene devices, semiconductor radiation detectors.**

Manuscript received June 3, 2011; accepted January 19, 2012. Date of publication January 31, 2012; date of current version May 9, 2012. The work of Y. P. Chen was supported by the Defense Threat Reduction Agency (DTRA) Young Investigator Program. The work of M. Foxe was supported by the Nuclear Forensics Graduate Fellowship Program which is sponsored by the U.S. Department of Homeland Security's Domestic Nuclear Detection Office and the U.S. Department of Defense's DTRA. This work was supported in part by the National Science Foundation, in part by the Department of Homeland Security, and in part by the Department of Defense under Award 0833689-ECCS, Award 2009-DN-077-ARI036-02, and Award HDTRA1-09-1-0047, respectively, and also in part by the U.S. National Science Foundation Directorate of Engineering and U.S. Department of Homeland Security's Domestic Nuclear Detection Office under the Project "Graphene-based ultrasensitive advanced radiation detectors" (GUARD), an "Academic Research Initiative" program. M. Foxe and G. Lopez made equal contributions to this paper. The review of this paper was arranged by Associate Editor P. J. Burke.

M. Foxe is with the Department of Mechanical and Nuclear Engineering, The Pennsylvania State University, PA 16802, USA (e-mail: mfoxe@psu.edu).

G. Lopez was with the School of Electrical Engineering, Purdue University, West Lafayette, IN 47907 USA, and with the Birck Nanotechnology Center, Purdue University, West Lafayette, IN 47907 USA. He is now with Sandia National Laboratories, Livermore, CA 94550 USA (e-mail: glopez@ecn.purdue.edu).

I. Childres is with the Department of Physics, Purdue University, West Lafayette, IN 47907 USA, and with the Birck Nanotechnology Center, Purdue University, West Lafayette, IN 47907 USA (e-mail: ichildre@purdue.edu).

R. Jalilian was with the Department of Physics, Purdue University, West Lafayette, IN 47907 USA and with the Birck Nanotechnology Center, Purdue University, West Lafayette, IN 47907 USA. He is now with NaugaNeedles, Louisville, KY 40299 USA (e-mail: romaneh_j@yahoo.com).

A. Patil is with the Department of Physics, Purdue University, West Lafayette, IN 47907 USA (e-mail: patil1@purdue.edu).

C. Roecker and J. Boguski are with the School of Nuclear Engineering, Purdue University, West Lafayette, IN 47907 USA (e-mail: croecker@purdue.edu; jboguski@purdue.edu).

I. Jovanovic is with the Department of Mechanical and Nuclear Engineering, The Pennsylvania State University, University Park, PA 16802 USA (e-mail: ijovanovic@psu.edu).

Y. P. Chen is with the Department of Physics, Purdue University, West Lafayette, IN 47907 USA, with the School of Electrical Engineering, Purdue University, West Lafayette, IN 47907 USA, and with the Birck Nanotechnology Center, Purdue University, West Lafayette, IN 47907 USA (e-mail: yongchen@purdue.edu).

Color versions of one or more of the figures in this paper are available online at http://ieeexplore.ieee.org.

Digital Object Identifier 10.1109/TNANO.2012.2186312

I. Introduction

HIGH-PERFORMANCE sensors for electromagnetic radiation such as light, X-rays, and γ-rays, and for particles such as energetic electrons and neutrons, are important for a multitude of scientific, commercial, and security applications. Among the major challenges in the development of radiation sensors for energetic ionizing radiation such as γ-rays and neutrons is achieving high-energy resolution at room temperature. We propose the utilization of the exceptional electronic properties of graphene (a single atomic layer of graphite) [1] to develop graphene-based radiation sensors.

We present the principles of operation for a graphene-based radiation detector (GRD), which utilizes an undoped absorber, with a focus on detection of γ-rays. Such detectors are of particular interest for detection of special nuclear material (SNM), one of the most important tasks for nuclear security. The modeled device architecture is a graphene field-effect transistor (GFET) [2], consisting of graphene on a radiation-absorbing, electrically gated, *undoped* semiconductor absorber, separated from graphene by a thin dielectric buffer layer. The technical approach is to utilize the sensitive dependence of the electrical conductivity of graphene on a local electric field, which can be abruptly changed by charge carriers produced by radiation in the underlying absorber material. This dependence, sharp even at room temperature, provides a unique opportunity to deploy graphene in conjunction with a variety of absorbers, with relaxed purity, carrier mobility, and lifetime constraints.

In our modeling work, we focus on the detection of γ-rays. Using Monte Carlo simulations (MCNP-Polimi [3]), the interactions of γ-rays with a thin Si absorber are modeled. The energy deposited and the location of energy deposition are calculated in configurations resembling common GFET devices. For the dominant mode of first interaction (Compton scattering), transport of energetic Compton electrons in the absorber is subsequently modeled using Monte Carlo Simulation of Electron Trajectory in Solids (CASINO) code [4]. The calculated ionized charge distribution is used as an input into a COMSOL Multiphysics model [5] to calculate the change in electric field, which results in the modulation of conductivity of graphene. Absorber material and dimensions used in the simulations discussed here are chosen to match current commonly fabricated GFETs (except that the substrates here are undoped, whereas the substrates used in conventional GFETs are doped) to emphasize the proof of principle. The simulation framework developed here can be extended to optimize the detector performance for specific applications, such as SNM detection.

1536-125X/$31.00 © 2012 IEEE

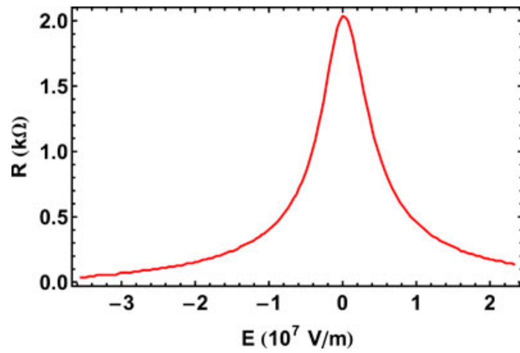

Fig. 1. Graphene exhibits a sharp peak "Dirac point" in resistance as a function of the electric field. The curve shown is based on representative experimental data measured in a GFET (see Fig. 2, with doped Si (10^{19} carriers/cm^3) as substrate and 300-nm-thick SiO_2 as buffer layer) at room temperature.

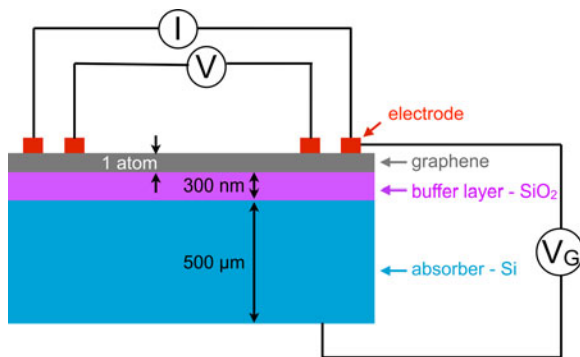

Fig. 2. A GFET consists of a gated undoped absorber (semiconductor), with an insulating buffer layer which serves as a gate dielectric. V_G is the gate voltage applied to the sample. Current is supplied across the graphene sample, and the voltage is measured to obtain the resistance of the graphene layer. Dimensions labeled are those typical of GFET devices commonly fabricated.

II. Graphene Field Effect Transistors

Graphene is a monolayer of graphite with unique electronic properties [1]. Graphene has a high carrier mobility, reaching 10 times or greater than that of Si at room temperature [2]. Graphene is a low-noise electronic material and has a resistance, which is very sensitive to local change of carrier density when graphene is near the charge neutrality point (see Fig. 1), or "Dirac point". This feature has been exploited to detect the adsorption/desorption of a single molecule on graphene [6]. It is proposed that the sensitivity of resistance to small changes in the electric field can be exploited to sense radiation. The sharpness of the resistance response of the graphene to the change of the external electric field suggests the possibility for its use as a high-gain preamplifier integrated into a GRD.

In our simulation of a prototype GRD based on a GFET, the graphene is coupled to a 500-μm-thick-gated undoped Si radiation absorber through a 300-nm-thick insulating buffer layer of SiO_2 (see Fig. 2). While one can use four metal electrodes on the graphene for accurate four-terminal resistance measurements, two-terminal measurements can be employed in many practical situations. An electric field is produced by applying a gate voltage between the back side of the absorber and one of the electrodes on graphene. The source and drain electrodes

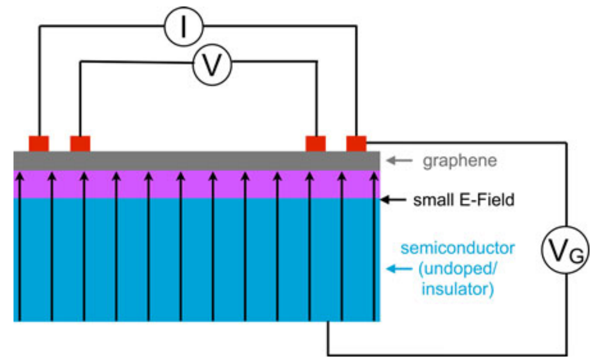

Fig. 3. When the undoped absorber acts as an insulator, the gate voltage V_G drops across both the absorber and the buffer layer, resulting in a relatively small electric field near graphene.

supply the current through the graphene and are used to measure the resistance of the graphene. The local electric field at graphene determines its resistance via the field effect, with this dependence most sensitive when the graphene is near its "Dirac point" (see Fig. 1) [2], [6].

III. Detecting the Presence of Radiation Without Charge Drift

A. Principle of Operation: Ionization-Induced Change of the Electric Field

The most common substrate used in a conventional GFET is a Si wafer with a thin-SiO_2 overlayer, where the Si is doped and used as the backgate. In the simplest scheme of employing a GFET to detect radiation, we instead use an *undoped*, gated absorber, so the electric field at the graphene can be significantly altered by the change of the conductivity of the absorber upon interaction with radiation. In general, using an undoped insulating (at sufficiently low temperature) semiconductor as the absorber, the gate voltage drops across both the absorber and the buffer layer (see Fig. 3, where the electric field is generated by a back-gate voltage).

Radiation interacting with the absorber results in ionization, which can increase the conductivity of the absorber, resulting in an electric field increase across the buffer layer (see Fig. 4). The change in electric field is indirectly sensed by measuring the resistance of graphene. This transient change in resistance could be used to detect the presence of radiation interacting with the absorber, and the magnitude of resistance change is related to both the total energy (ionized charges) deposited in the absorber and the location of the ionized charges (see Section III-C).

B. Monte Carlo Modeling for Radiation Interaction

We used the absorber material (Si, except being undoped) and dimensions of common GFETs (see Fig. 2) for our simulations. Using MCNP-PoliMi [3], we modeled the irradiation of a GFET with a 1-MeV γ-ray source located 1 cm from the bottom of the absorber, and centered on the axis defined by graphene. The energy deposited and the position of interaction were calculated in the simulation. From the energy deposited, we modeled the

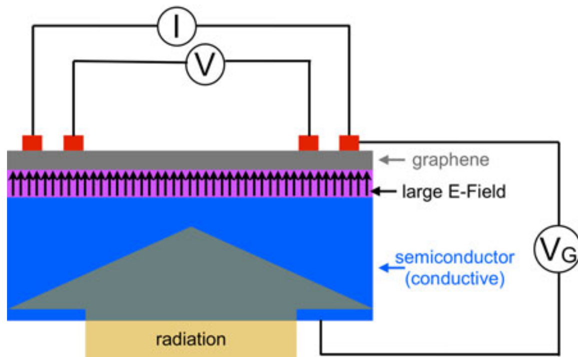

Fig. 4. The incoming radiation ionizes the undoped semiconductor to create a conducting absorber. The gate voltage V_G is now effectively "transferred" through the absorber and drops across the buffer layer. This results in an increased electric field which is detected by graphene via the field effect (see Fig. 1) and is signaled by a corresponding change in resistance. In the simplistic schematic shown here, the entire absorber is assumed to be ionized. In practice, the ionization is generally spatially nonuniform and the change of electric field depends on the amount and location of ionized charges.

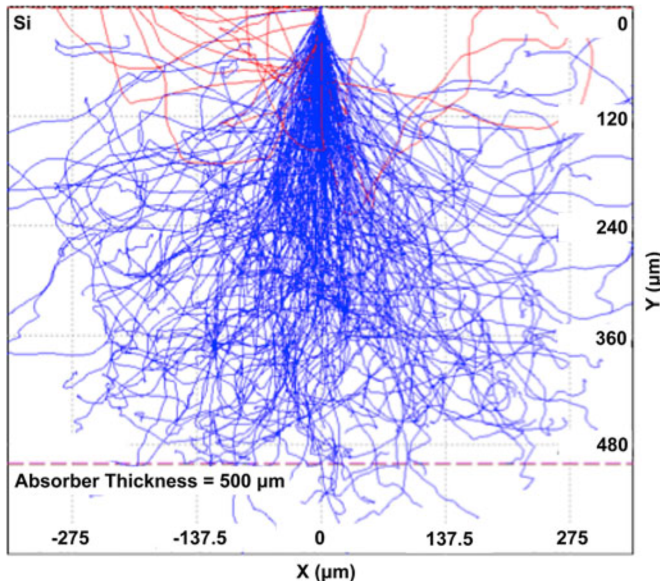

Fig. 5. CASINO simulation of a beam of 400-keV electrons being emitted normal to a Si wafer (thickness = 500 μm in typical devices presently fabricated), representative of Compton electrons generated from γ-ray interactions in the absorber. The red tracks are the trajectories of electrons which have been backscattered out of the absorber. The origin (0,0) marks the entry point of the electrons.

Compton electron trajectories within the Si absorber using the CASINO code [4]. CASINO simulation shows a wide variation in electron trajectories characteristic for electron stopping (see Fig. 5).

As a first-order approximation, we assume that the electron track is straight and split each electron track into two ionization regions with constant, but different specific ionizations. The first ionization region represents the beginning of the electron track, while the second ionization region represents the vicinity of the Bragg peak, with a peak-to-tail specific ionization ratio calculated from CASINO. The CASINO simulations show a significant fraction of electrons escaping the Si absorber of standard wafer thickness (500 μm) once they reach energies above ~400 keV.

C. COMSOL Model for Electronic Response

In conjunction with the MCNP modeling, finite element method (FEM) simulations were conducted in order to estimate the electric field distribution in a model of the proposed GRD. The FEM platform utilized in the simulations was COMSOL Multiphysics 3.5a in the "conductive media dc" mode for two dimensions. Laplace's equation was solved in the model

$$\nabla \cdot (\sigma \nabla V) = 0 \tag{1}$$

where σ is conductivity and V is voltage. The specific simulation results here are obtained assuming an electron mobility μ_e of 1413 cm^2/V/s, a hole mobility μ_h of 470 cm^2/V/s, and a value of conductivity for Si of 5.1×10^{-10} S/m (which can be obtained, for example, in a lightly doped Si at 10 K with phosphorus doping of $N_D = 10^{15}$ cm^{-3}). The insulating oxide layer has a conductivity value of 1×10^{-12} S/m. Si is chosen in this example as it is the type of substrate material used in most currently fabricated GFETs [2]. Similar results based on the same operational principle are expected for other undoped/lightly doped semiconductor absorbers with sufficiently low background conductivity, achieved either at low temperatures, or using wider bandgap semiconductors, in which case low temperatures may not be needed for operation.

Our 2-D device model consists of a square Si absorber, measuring 500 μm × 500 μm (width × thickness), with a rectangular SiO_2 buffer layer, measuring 500 μm × 300 nm. The backgate of the GFET structure is located on the bottom of the Si absorber, while the graphene region is modeled as the grounded top portion of the insulating SiO_2 layer. We use insulating boundary conditions and continuity across interfaces in our model. A triangular mesh of approximately 2×10^4 elements is generated for the simulation.

The simulation investigates the modulation of the electric field due to the generation of charges in the undoped Si absorber following a 400 keV of energy deposition. Carrier concentration data generated by the MCNP-Polimi and CASINO simulations are used to determine the conductivity of the ionized regions in the model. The conductivities of ionization regions are 266×10^{-3} and 58×10^{-3} S/m for the beginning and end of the ionization track, respectively. The backgate is biased at 10 V in the model. Fig. 6 illustrates the effect of the presence of ionization regions on the distribution of the equipotential lines in the Si absorber for a representative energy deposition profile with two different starting locations.

In the simulation, the change of electric field strength in the SiO_2 just below the graphene and above the ionized absorber region can be on the order of 10^7 V/m for the energy deposition profile and magnitude used in the model. An electric field change as large as that suggested by the simulation is capable of modulating the number of charge carriers in graphene to produce a measurable change of resistance (see Fig. 1), on the order of 100Ω–1 kΩ.

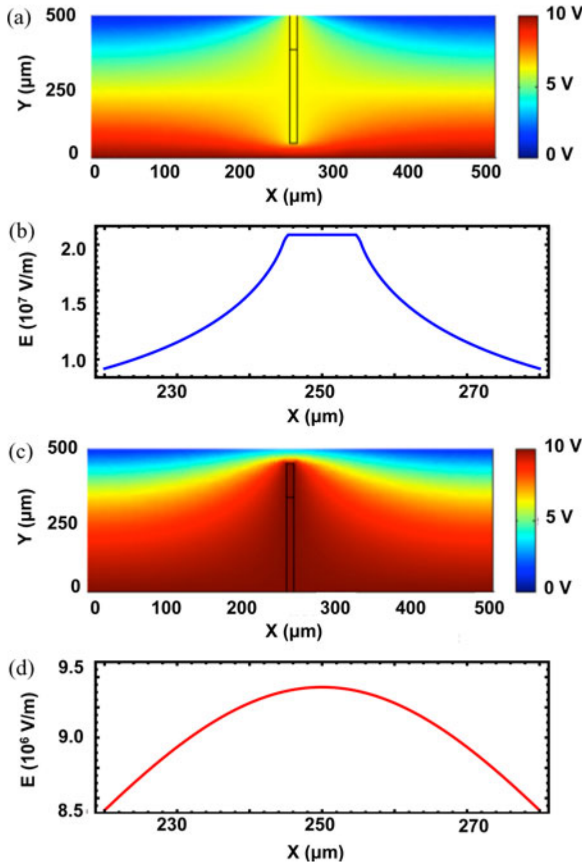

Fig. 6. (a) and (c) Calculated potential and (b) and (d) electric field profile 1 nm below the SiO_2 top surface (near graphene) for two examples of ionization regions that differ only in position. (a) and (b) Representative energy deposition profile reaches the Si/SiO_2 interface; (c) and (d) it starts from the back surface of the substrate and terminates 50 μm below the surface. The backgate is biased at 10 V, while the top SiO_2 layer is at a ground potential. The uniform thickness of 10 μm and profile of the ionization region are selected for ease of simulation. Realistic ionization tracks would have more complicated profiles (see Fig. 5).

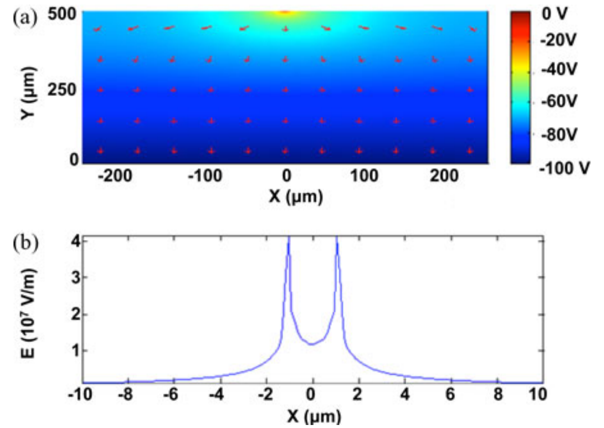

Fig. 7. (a) COMSOL simulation of the field lines created with a gate voltage of $V_G = -100$ V, applied from the electrode on the bottom of the absorber to the graphene (taken to be 2-μm wide in this simulation). The field lines, shown as red arrows, reveal the path of the drifted electrons (note that the electron velocity is opposite to the arrows), which converge under the graphene, independent of their initial position. (b) The line plot shows the electric field strength 5-nm below the SiO_2 layer, about the graphene center axis.

IV. Detection With Energy Resolution: Drifting Charges

A. Principle of Operation

While the simple scheme described above could be used to detect the presence of radiation, in many applications such as SNM detection it is paramount to accurately measure the energy of the radiation deposited in the absorber. In single-event radiation sensing, the absorber is ionized nonuniformly, and the spatial distribution of charge deposition is highly random (see Section III, Fig. 5). As a result, the electric field change near graphene has a poor correlation with the energy deposited in the absorber, which would compromise the ability to measure deposited energy through the change of resistance. An example can be seen in Fig. 6, where the same amount of energy deposited in different locations would lead to very different responses in graphene. This issue can be addressed by drifting the charge to the top surface of the absorber, effectively normalizing the position of each interaction to the layer with a constant distance (the thickness of the SiO_2 buffer layer) from graphene. This drift can be accomplished by applying the electric field between the electrically biased back-gate electrode (at the back of absorber) and the top electrode (graphene). In a typical GFET, the back surface gate electrode is much larger than the graphene, creating curved electric field lines, with electric field magnitude increasing with reduced distance to the graphene (see Fig. 7). The field lines "funnel" electrons created by the radiation in the absorber to the location directly under the graphene, resulting in an electric field response independent of where these ionized charges are originally produced in the absorber (see Fig. 8). The net change of the electric field applied to graphene is now dependent only on the amount of charge, effectively correlating it with the deposited energy.

In the GRD described above, the insulating SiO_2 layer prevents the drifted electrons from flowing into the graphene. Since the electrons accumulate under the buffer layer, the final and maximum change in electric field experienced by the graphene (after all electrons created in one radiation interaction event are drifted under the graphene), will be measured by the change of graphene resistance, and is directly related to the number of electrons created. If "reset" of the sensor is required in preparation for subsequent measurements, the electrons can be drained through the auxiliary source and drain electrodes.

Consider a GRD which has a graphene with an area of 100 μm^2 and an absorber with an area of 1 cm^2 and thickness t_a of 500 μm. Such a large aspect ratio (ratio of width to thickness) of the absorber results in a significant variation of the strength of the electric field throughout the absorber. We found that the variation in electric field strength results in a difference in carrier drift times of $\sim$6 orders of magnitude between the centerline and the outer edge of the absorber (see Fig. 9).

For electrons starting at $x \approx 2t_a$, the recombination probability is $\sim 0.1\%$, given a recombination time of 10^{-3} s and back-gate voltage of -100 V. When the starting position is increased up to $x \approx 4t_a$, recombination occurs for $\sim 1\%$ of the electrons (see Fig. 10). This suggests that it is desirable that

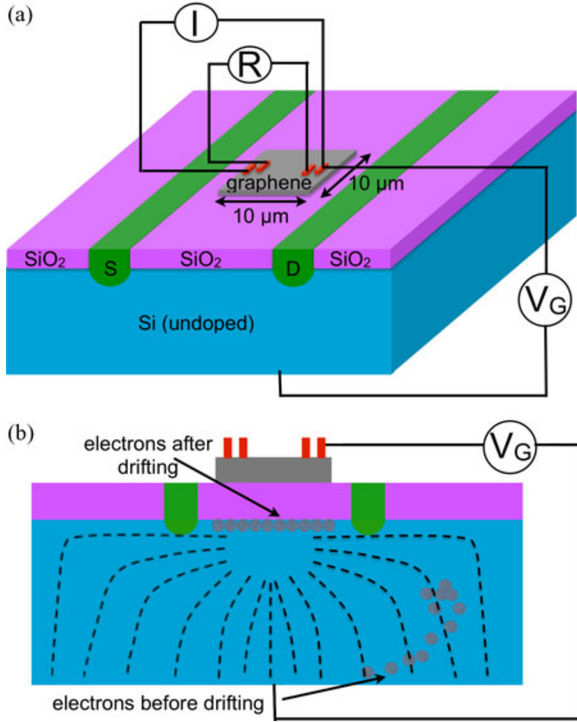

Fig. 8. (a) We consider a GRD, where the typical size of the graphene electrode is smaller than the size of the underlying absorber. Electric field lines are generally curved and direct the electrons toward the location directly under the graphene. With all electrons accumulated under the buffer layer, the electric field change measured by the change in graphene resistance is directly proportional to the number of electrons created by ionization. (b) shows the crosssection of a GRD showing electrons both before and after they are drifted. The electron trajectories are along the electric field, whose direction is represented by the dashed lines.

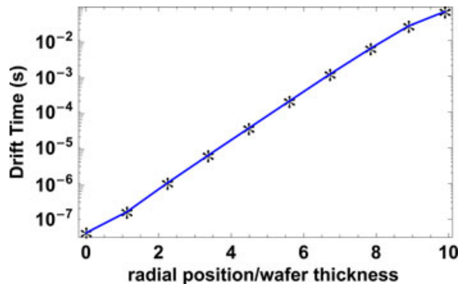

Fig. 9. As the starting position of the electron moves away from the axis defined by the graphene, the drift time increases exponentially. The drift time varies by 6 orders of magnitude over a radial distance of 5 mm for a 500-μm-thick Si absorber. The electron starting position is $y = 10$ μm, with the graphene surface at $y = 500$ μm (here y-direction is perpendicular to graphene and the back surface of absorber is at $y = 0$). This simulation is performed for a backgate voltage is -100 V and a graphene size of 10 μm $\times$ 10 μm.

the absorber (for a given graphene size) have a low aspect ratio (width/thickness) to achieve high-energy resolution and speed (see Section IV-B). For example, with an aspect ratio of $\sim$2, the electron drift time for the GRD simulated above is no more than $\sim$200 ns, resulting in a maximum operating speed of 5 MHz. To reduce the aspect ratio, one may increase the thickness of the substrate or decrease the available lateral size of the detector (eg. using etching to segment the detector).

To adapt the proposed architecture to larger thicknesses and different absorbers, the voltage applied may have to be altered for two reasons. First, the increased thickness of the absorber may require additional voltage to maintain the same electric field. Second, absorbers that are desirable for other reasons may have different electron and hole mobilities and recombination lifetimes, thus, requiring a change in electric field for the same drift time and percentage of recombined electrons.

B. Energy Resolution

Energy resolution is the key performance parameter when considering the use of a GRD in γ-ray spectroscopy such as that needed for SNM detection. Contributions to the finite energy resolution of the GRDs include both the intrinsic (Poissonian) fluctuation of the number of charge carriers produced for a given deposited energy, and the limitations of the detector architecture, including the effects such as charge trapping [7], loss of charge to auxiliary electrodes, and the noise in the measurement of graphene resistance.

A simple estimate of the expected maximum energy resolution in a GRD with a Si absorber is provided, and the relevant contributions to the resolution limit are illustrated in Fig. 11 for an example with representative parameters. The energy resolution is calculated for all contributions to the finite energy resolution, and the total energy resolution is calculated by adding each contribution in quadrature multiplied by 2.35, given that each contribution is Gaussian.

Poisson statistics governing the ionization process results in an energy resolution of $\sqrt{F/N}$, where N is the number of charge carriers in the absorber given a W-value of 3.65 eV [8], and the Fano factor of Si, $F = 0.115$ [9]. Assuming an electron mobility and lifetime product $(\mu_e \tau_e) > 1$, and charge trapping to be a linear function of distance [10], we do not include charge trapping in the energy resolution calculations. The energy resolution due to recombination is assumed to be proportional to the fraction of electrons lost through recombination; to achieve a recombination contribution to the resolution of 0.01%, an aspect ratio of $\sim$1 is required. The error increases to $\sim 0.1\%$ when the aspect ratio is increased to 2. To calculate the energy resolution due to noise associated with the measurement of graphene resistance, we assume that each electron generated in the absorber corresponds to one induced in the graphene, and use the correlation between the charge carrier density induced in graphene and graphene resistance. The relation between graphene's charge density and resistance can be obtained from Fig. 1, and the relationship between the E-field and carrier density can be obtained from

$$E\, t_b \frac{\epsilon_r \epsilon_o}{q\, t_{\text{buffer}}} = n \tag{2}$$

where E is the electric field, t_b is buffer layer (SiO_2) thickness, ϵ_r is the relative permitivity of SiO_2, ϵ_o is the permitivity of free space, q is the electron charge, and n is the charge carrier density of graphene. With $N_R = \delta R^2/R^2$ estimated to be $\lesssim 15 \times 10^{-8}$, based on prior measurements [11], we calculate the associated maximum charge density error by dividing the error in resistance measurement by the derivative of the Dirac curve $(\delta R/\delta n)$ at

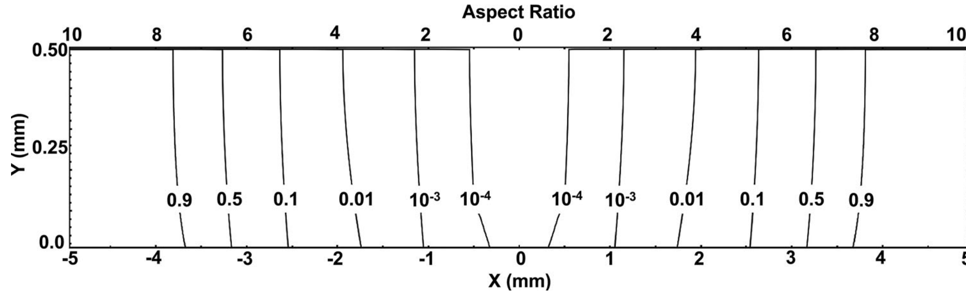

Fig. 10. Probability of an electron born at the given location within the absorber to undergo recombination. A recombination time of 10^{-3} s and back-gate voltage of -100 V are used for this calculation, and a graphene layer with a lateral size of 10 μm is centered at (0 and 0.5 mm). If electrons are produced at $\sim$2 times the wafer thickness (1 mm) away from the detector vertical centerline, recombination occurs for 0.1% of the electrons. At $\sim$4 times, the thickness (2 mm) away from the detector vertical centerline, recombination occurs for 1% of the electrons.

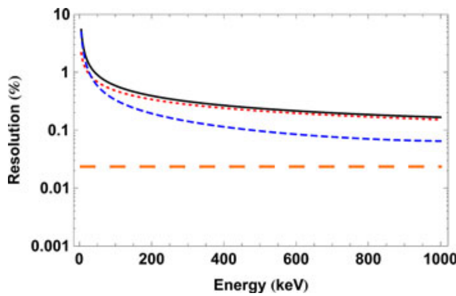

Fig. 11. Calculated GRD energy resolution as a function of deposited energy, with a Si absorber and an initial electric field of 2×10^5 V m^{-1}. Total energy resolution (black solid) is obtained by quadrature addition of the component of energy resolution due to Poisson statistics (red dotted), the component of energy resolution due to graphene resistance noise (blue dashed), and the component of energy resolution due to carrier recombination (orange long-dashed) of 0.01% for an aspect ratio of $\sim$1 (see Fig. 10).

the calculated resistance for complete energy deposition

$$\frac{\delta n\ A_g}{U/W} = \eta \tag{3}$$

where

$$\delta n = \frac{\sqrt{\frac{\delta R^2}{R^2}}R}{\frac{\delta R}{\delta n}} \tag{4}$$

R is resistance calculated for charge density due to U/W electrons, n is charge carrier density of graphene, A_g is area of the graphene (100 μm^2), $W = 3.65$ eV for Si, U is the energy deposited, and η is energy resolution associated with resistance measurement noise in graphene. Two competing effects affect the predicted energy resolution of the GFET operating on the negative slope of the Dirac curve (see Fig. 1). As the deposited energy increases, the graphene resistance is reduced, thus, decreasing the error in the resistance measurement. On the other hand, as the deposited energy increases, the slope of the Dirac curve decreases, resulting in a greater error in the measurement of charge density for the same error in resistance. For energies above $\sim$50 keV, the dominant effect determining the total energy resolution is the Poissonian fluctuation in the number of ionized charges.

While the above calculations are made for a representative graphene size of 10 μm $\times$ 10 μm, by changing the size of the graphene, the electric field curvature pattern in the absorber and the dynamic range of the GRD can be altered, with a concomitant change in the graphene energy resolution due to recombination fraction and resistance measurement error. With chemical-vapor-deposition-based graphene fabrication [12], [13], the size of graphene can be optimized for a variety of energy ranges and detector sizes, with promise for achieving high-energy resolution with large-area GRDs.

V. Discussion and Conclusion

Graphene-based sensors have a potential to provide a novel, unique mechanism for detection of radiation. The sharp change in resistance as a function of the external electric field allows the graphene to act as a built-in preamplifier. We can also view the GRD as an (indirect) photoconductor with high gain of transconductance due to the sharp field effect in graphene. Compared with more conventional detector architectures based on charge sensing, the effective decoupling of the detector (graphene) and the absorber (substrate) in the GRD could offer potential benefits by allowing more flexibility in the choice of the absorber material, and its size in designing GRDs.

In addition, the proposed GRD utilizes the unique material properties of graphene to provide several potential operational advantages over conventional MOSFET (which can also be utilized as radiation sensors). Graphene exhibits an ultralow electrical noise, which can otherwise limit the sensitivity of conventional detectors [6]. Graphene's high electrical conductivity and pristine crystallographic nature allow for the reduction of Johnson and pink $(1/f)$ noise [6], [14] from degrading acquired signals. Low noise is retained throughout graphene's conductivity range, including "Dirac point", where resistivity is at a maximum (but finite, while a conventional MOSFET resistance would diverge when depleted), as well as during ambipolar operation in n-type or p-type regimes [1].

GRD also brings the potential of very high-speed operation. Dual-gated GFETs have been shown to produce cutoff frequencies as high as 300 GHz, much higher than the cutoff frequency obtainable in Si MOSFETs of comparable size [15], [16]. Graphene can be deposited or transferred on a number of absorbers, allowing for the incorporation of a variety of semiconductors in the device architecture with less stringent requirement on the absorber purity or carrier mobility and lifetime.

ACKNOWLEDGMENT

The authors would like to acknowledge helpful discussions with Prof. S. Luryi and Dr. I. Hau.

REFERENCES

[1] A. K. Geim and K. S. Novoselov, "The rise of graphene," *Nat. Mater.*, vol. 6, no. 3, pp. 183–191, Mar. 2007.
[2] K. Novoselov, A. Geim, S. Morozov, D. Jiang, Y. Zhang, S. Dubonos, I. Grigorieva, and A. Firsov, "Electric field effect in atomically thin carbon films," *Science*, vol. 306, no. 5696, pp. 666–669, Oct. 2004.
[3] S. Pozzi, E. Padovani, and M. Marseguerra, "MCNP-polimi: A monte-carlo code for correlation measurements," *Nucl. Instrum. Methods A*, vol. 513, no. 3, pp. 550–558, Nov. 2003.
[4] P. Hovington, D. Drouin, and R. Gauvin, "Casino: A new monte carlo code in C language for electron beam interaction—Part 1: Description of the program," *Scanning*, vol. 19, no. 1, pp. 1–14, Jan. 1997.
[5] COMSOL Multiphysics 3.5, (2008). [Online]. Available: http://www.comsol.com
[6] F. Schedin, A. K. Geim, S. V. Morozov, E. W. Hill, P. Blake, M. I. Katsnelson, and K. S. Novoselov, "Detection of individual gas molecules adsorbed on graphene," *Nat. Mater.*, vol. 6, no. 9, pp. 652–655, Sep. 2007.
[7] Z. He, G. Knoll, D. Wehe, and J. Miyamoto, "Position-sensitive single carrier cdznte detectors," *Nucl. Instrum. Methods A*, vol. 388, no. 1–2, pp. 180–185, Mar. 1997.
[8] N. Tsoulfanidis, *Measurement and Detection of Radiation*. New York: Taylor & Francis, 1986, p. 249.
[9] G. Lutz, *Semiconductor Radiation Detectors—Device Physics*. Berlin, Germany: Springer-Verlag, 1996, p. 80.
[10] P. Luke and E. Eissler, "Performance of cdznte coplanar-grid gamma-ray detectors," *IEEE Trans. Nucl. Sci.*, vol. 43, no. 3, Part 2, pp. 1481–1486, Jun. 1996.
[11] A. N. Pal and A. Ghosh, "Ultralow noise field-effect transistor from multilayer graphene," *Appl. Phys. Lett.*, vol. 95, no. 8, pp. 082105-1–3, Aug. 2009.
[12] X. Li, W. Cai, J. An, S. Kim, J. Nah, D. Yang, R. Piner, A. Velamakanni, I. Jung, E. Tutuc, S. K. Banerjee, L. Colombo, and R. S. Ruoff, "Large-area synthesis of high-quality and uniform graphene films on copper foils," *Science*, vol. 324, no. 5932, pp. 1312–1314, Jun. 5, 2009.
[13] H. Cao, Q. Yu, L. A. Jauregui, J. Tian, W. Wu, Z. Liu, R. Jalilian, D. K. Benjamin, Z. Jiang, J. Bao, S. S. Pei, and Y. P. Chen, "Electronic transport in chemical vapor deposited graphene synthesized on cu: Quantum hall effect and weak localization," *Appl. Phys. Lett.*, vol. 96, no. 12, pp. 122106-1–3, Mar. 22, 2010.
[14] Y.-M. Lin and P. Avouris, "Strong suppression of electrical noise in bilayer graphene nanodevices," *Nano Lett.*, vol. 8, no. 8, pp. 2119–2125, Aug. 2008.
[15] L. Liao, Y.-C. Lin, M. Bao, R. Cheng, J. Bai, Y. Liu, Y. Qu, K. L. Wang, Y. Huang, and X. Duan, "High-speed graphene transistors with a self-aligned nanowire gate," *Nature*, vol. 467, no. 7313, pp. 305–308, Sep. 2010.
[16] Y.-M. Lin, H.-Y. Chiu, K. A. Jenkins, D. B. Farmer, P. Avouris, and A. Valdes-Garcia, "Dual-gate graphene fets with f(t) of 50 ghz," *IEEE Electron. Devices Lett.*, vol. 31, no. 1, pp. 68–70, Jan. 2010.

Authors' photographs and biographies not available at the time of publication.